# Hydraulic characterization of settled sediment layer and subsoil in an urban infiltration basin

Caractérisation hydraulique d'une couche sédimentaire et du sol sous-jacent en fond de bassin d'infiltration urbain

Lassabatere L.*, Angulo-Jaramillo R.**-***, Winiarski, T**, Delolme, C**

* Division for water, LCPC, Route de Bouaye, 33431 Bouguenais cedex

** Laboratory of Environmental Sciences (LSE), ENTPE, Rue Maurice Audin, 69518, Vaulx-en-Velin, France

*** LTHE, BP 53, 38041 Grenoble cedex 9, France

## RESUME

L'impact de la couche sédimentée en fond de bassin d'infiltration sur sa capacité à infiltrer l'eau est testée par infiltrométrie. Une caractérisation hydraulique complète est proposée, couplant la modélisation des données d'infiltration avec l'algorithme BEST avec des essais de séchage d'éprouvettes de matériaux en laboratoire. La réduction de la capacité d'infiltration du bassin résulte de la faible conductivité hydraulique saturée du sédiment et de sa forte hydrophobicité (matières organiques). La caractérisation hydraulique complète du sédiment et du sol servira pour la modélisation numérique de l'infiltration d'eaux pluviales dans le bassin de Cheviré pour divers scenarii.

## ABSTRACT

The impact of a sedimentary layer on the infiltration capacity of an infiltration basin was studied through infiltration experiments. The combination of the modeling the infiltration experiments using BEST algorithm with laboratory soil column evaporation experiments helped to estimate unsaturated hydraulic characteristics of the materials. Poor infiltration capacities of the basin were the result of the combined effect of the sediment low hydraulic conductivity and high hydrophobicity (organic matter). The complete hydraulic characterization of the materials will constitute a material database useful to the numerical modeling of stormwater infiltration in Cheviré basin for several scenarii of monitoring.

## KEYWORDS

Beerkan method ; hydraulic characteristics ; hydrophobicity ; infiltration basin ; sediment.

# 1 INTRODUCTION

The development of impermeable urban areas has increased the volumes of stormwater necessitating alternative techniques to be restituted to the soil (Valiron and Tabuchi, 1992; Chocat et al., 1999). One of these alternatives consists in discharging runoff waters into specific works such as infiltration basins or pits. These basins require a good monitoring to avoid dysfunction in term of quantity and quality. Stormwater carry out lots of contaminants and suspended solids that tend to accumulate in infiltration basins and form a sedimentary layer covering the subsoil. In such a context, there is a need for knowledge concerning the impact of such a layer on stormwater infiltration and on the transfer of pollutants carried out by stormwater.

The study of water infiltration in unsaturated soils requires the estimation of two hydraulic characteristic curves. The water retention curve, $h(\theta)$, which relates volumetric water content, $\theta$, with water pressure head, h, and the hydraulic conductivity curve, $K(\theta)$, which characterizes the material ability to transport water under a unit hydraulic gradient. Several methods have been developed to determine these hydraulic characteristic curves. Recently the proposed Beerkan method (Braud et al., 2005), offers a complete hydraulic characterization from simple soil particle size analysis and in situ infiltration experiments. This method was successfully used to study different soils through the "BEST" for "Beerkan Estimation of Soil Transfer parameters" algorithm (Lassabatère et al., 2006). In BEST, water retention and hydraulic conductivity curves are described with the analytic formulations of van Genuchten with Burdine conditions and Brooks and Corey with Burdine capillary model, respectively (Burdine, 1953; Brooks and Corey, 1964; van Genuchten, 1980):

$$\frac{\theta-\theta_r}{\theta_s-\theta_r}=\left(1+\left(\frac{h}{h_g}\right)^n\right)^{-m} \quad (1\text{ a})$$

with

$$m=1-\frac{2}{n} \quad (1\text{ b})$$

$$K_r(\theta)=\frac{K(\theta)}{K_s}=\left(\frac{\theta-\theta_r}{\theta_s-\theta_r}\right)^{\eta} \quad (2\text{ a})$$

$$\eta=\frac{2}{m\,n}+3 \quad (2\text{ b})$$

The aims of the paper are (1) to characterize the impact of the sedimentary layer on the infiltration capacity of the Cheviré infiltration basin and (2), to bring explicative information through the unsaturated hydraulic characterization of both the subsoil and the sedimentary layer. Hydraulic characterization of both materials was performed using both BEST in-situ infiltration method and evaporation-based laboratory experiments.

# 2 MATERIAL AND METHODS

## 2.1 Cheviré infiltration basin

The infiltration basin is located near Nantes (France). It collects and infiltrates the runoff water from 38425 $m^2$ of the Cheviré bridge into a sandy soil on 720 $m^2$ infiltration surface. The basin is 15 years old, leading to the settlement of a sedimentary layer (a loamy-clay material) over the sandy soil. The sedimentary layer thickness varies from a few cm at the border of the basin to more than 30 cm at the center.

Measurements and infiltration experiments were performed at reference sites (sandy soil at basin borders) and at several places with various thickness of the sedimentary layer (2 cm, 5 cm and 30 cm) (Figure 1). These were also performed for the subsoil, at a 30 cm depth, except when the sedimentary layer was more than 5 cm thick. Locations are referred according to the material (sand or sediment) and to the sedimentary layer thickness ("$S_{sand}$" for the reference location and "$S_{sed\_xcm}$" for locations where x cm of sedimentary layer settled over the sandy soil).

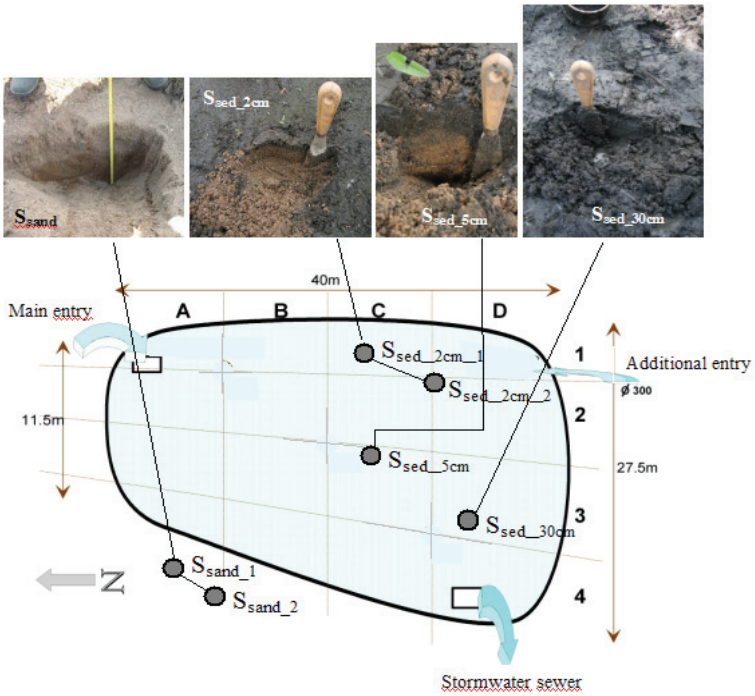


Figure 1 : Cheviré basin and infiltration experiment locations.

## 2.2 *In situ* Beerkan infiltration experiments

The protocol for the Beerkan method uses a simple annular ring 9.5 cm in diameter and 7 cm in height installed just below the ground surface. Measured doses of water of the same volume are prepared. The first dose is poured into the ring and the time required for infiltration of the dose is measured. This represents one data point. The second dose is then poured into the ring and the procedure repeated to get the second data point. The procedure is repeated until a sufficient number of data points have been collected such that the infiltration rate has reached steady-state. The data set is made up of a number of discrete points through which the fitting infiltration curves are passed (Lassabatère et al., 2006). From the geometric configuration, it is then assumed a three-dimensional infiltration at null pressure head, i.e. saturated volumetric water content, applied at soil surface.

The infiltration capacity ($L_{10cm}$) is calculated, from cumulative infiltrations, as the ratio between 10 cm height of cumulative infiltration and the corresponding time ($t_{10cm}$):

$$L_{10cm} = \frac{10\,cm}{t_{10cm}} \quad (3)$$

When the total infiltrated height is less than 10 cm, the infiltration capacity was defined as the ratio between the total infiltrated height against the total duration of the experiment.

Near infiltration locations, a ring (5.7 cm in diameter and 10 cm in length) was driven into the soil to sample undisturbed *in situ* materials. Depending upon the locations, the sampled materials differed: sand at reference locations $S_{sand}$ and all locations under the sedimentary layer, sediment at location $S_{sed\_30cm}$, mixture of 8 cm of sand with 2 cm of sediment at locations $S_{sed\_2cm}$, mixture of 5 cm of both sand and sediment at location $S_{sed\_5cm}$. The samples were then air-dried and homogenized to determine both initial water contents and dry bulk densities. Porosities were calculated by assuming an average solid specific density of 2.65 g $cm^{-3}$. Particle size analyses were performed on the fraction less than 2 mm through simple sieving and verified through laser particle size analysis for the fraction less than 1 mm.

### 2.3 Laboratory determination of water retention curves

Water retention curves were experimentally determined for both sediment and sand. The sediment and sand were packed in columns (14 cm in diameter and 10 cm height) with water contents of 25% and 10%, and dry bulk densities of 0.80 g $cm^{-3}$ and 1.70 g $cm^{-3}$ (i.e. porosities of 69% and 40%), respectively. The columns were saturated during 24 hours, and then submitted to a fan-forced evaporation at room temperature. During evaporation, volumetric water contents and water pressure heads were measured using capacity cells and mini-tensiometers, respectively. Experimental retention curves were then built by simple correlation between volumetric water content and water pressure head values.

## 3 RESULTS

### 3.1 *In situ* bulk parameters

The average dry bulk density of the sediment was determined at the center of the basin (location $S_{sed\_30cm}$), and ranged 0.342 g $cm^{-3}$ +/- 0.016 g $cm^{-3}$. This corresponds to a large porosity, 87.1% +/- 0.6%. The fine fraction, e.g. $d < 200$ μm, was predominant with a fine fraction content ($F_{200\mu m}$) higher than 95%. The particle size distribution is well graded with a mean diameter of 50 μm (Figure 2a, sediment).

The soil and the subsoil (under the sedimentary layer) correspond to the same sandy soil. Nevertheless, the mean dry bulk density is relatively low, i.e. 0.843 g $cm^{-3}$ +/- 0.060 g $cm^{-3}$ (mean porosity 68.2% +/- 2.3%). The coarse fraction (200 μm < d < 2 mm) was predominant ($F_{200\mu m} < 5\%$). Sand particle size distribution is narrow-graded and coarse with an averaged diameter of 650 μm (Figure 2a, sand).

At the other locations ($S_{2cm}$, $S_{5cm}$), particle size distribution and bulk densities were determined for the mixtures sand / sediment constituting the sampled materials. The sediment and the sand could be separated from the mixtures through sieving at 200 μm. The fine fraction contents ($F_{200\mu m}$) of the mixtures quantify the sediment content in the mixtures. This is a good indicator of the sand "contamination" by the sediment. Figure (2a) shows the good correspondence between the particle distributions of the sand and the sediment obtained from the mixtures and their reference particle size distributions obtained at locations $S_{sand}$ and $S_{sed\_30cm}$ (Figure 2a, lines against the curve "sediment" and "sand"). Figure 2b shows the decrease in bulk density with sediment content ($F_{200\mu m}$) from the values of sand (low $F_{200\mu m}$) down to the values of sediment (high $F_{200\mu m}$).

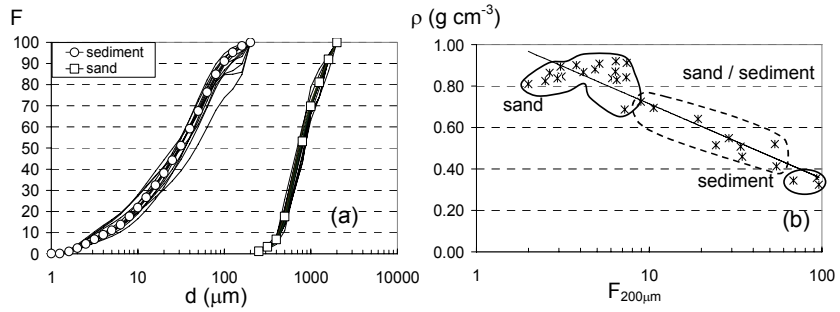


Figure 2 : Particle size distributions of the fine (d < 200 μm) and coarse (200 < d <2000 μm) fractions for sand, sediment and mixtures sand / sediment (a), correlation between dry bulk densities (ρ) and fine fraction contents ($F_{200\mu m}$) (b).

## 3.2 Infiltration capacity and hydrophobicity

Infiltration results are similar for the sandy soil at reference locations and under the sedimentary layer but they depend on soil initial water content. At high initial water contents, infiltration capacities ranged from 4 and 12 cm $min^{-1}$ (Figure 3a, wet sand). Cumulative infiltrations show a linear behavior (Figure 3b, wet) which is representative of a steady state quickly reached that means a 1D water flow pattern mainly gravity driven. Then, steady state infiltration rates can be approximated by (Smith et al., 2002):

$$q_{+\infty} \approx K_s \qquad (4)$$

where $K_s$ is the saturated hydraulic conductivity. Steady state infiltration rates can thus be considered as good estimators of saturated hydraulic conductivities.

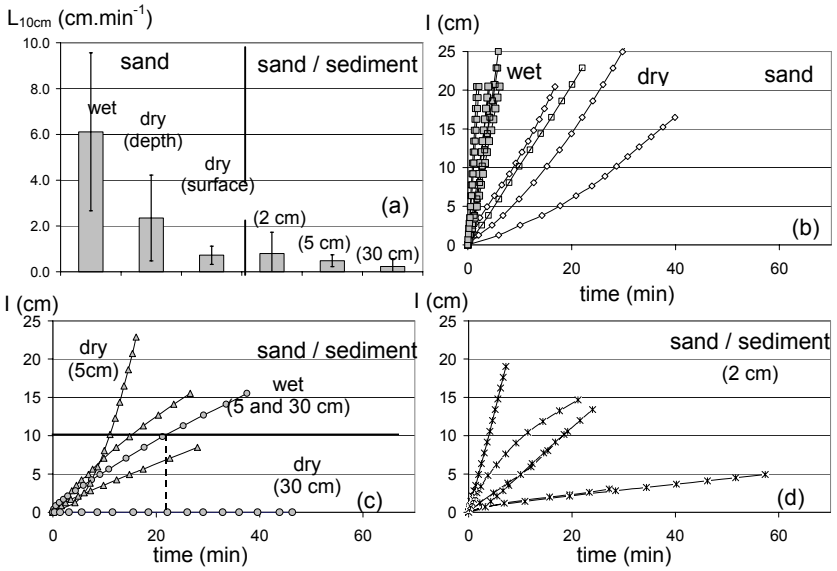


Figure 3 : Infiltration capacity vs. sedimentary layer thickness (a); Beerkan Method cumulative infiltrations on the sand (b) and on the sedimentary layer above the sand (c, d).

At lower initial water contents, infiltration capacities of the same sandy soil decreased (Figure 3a, dry sand). In such a case, cumulative infiltrations were no longer linear and presented a particular convex shape (Figure 3b, dry). The increase in slope of cumulative infiltration curves with time reveals the increase in infiltration rates when the material gets wetter. This behavior is representative for hydrophobicity (Wang et al., 2000; Robichaud, 2000). Hydrophobicity can result from the significant organic matter content of the sandy soil near the surface (TOC = 1.4 g $kg^{-1}$), due to significant organic activity (plants, animals, bacteria, etc.) (Buczko et al., 2002, Mataix-Solera and Doerr, 2004).

The presence of the sedimentary layer above the sand greatly decreased infiltration capacities to less than 1 cm $min^{-1}$, whatever the thickness of the sedimentary layer and water contents (Figure 2a, sand / sediment). This significant reduction may have resulted from the specific hydraulic characteristics of the sedimentary layer. When the sediment was initially wet, cumulative infiltrations presented a usually observed concave shape with a decrease in infiltration rates with time (Figure 3c, wet). The shapes of infiltration curves show that the flow was initially capillary driven and subsequently both capillary and gravity driven (Smith et al., 2002). Steady states were not reached as quickly as observed for sand experiments. In such cases, the infiltration rates can not be directly linked to saturated hydraulic conductivities. BEST algorithm was then used to fit cumulative infiltrations and led to both accurate modeling and plausible values for saturated hydraulic conductivities (data not shown).

When the sedimentary layer was initially dry, cumulative infiltrations presented a specific convex shape, even more marked than for the dry sand (Figure 3c, dry (5 cm)). This highlights the strong hydrophobic behavior of the sediment (Wang et al., 2000, Clothier et al., 2000). For 30 cm, hydrophobicity was strong enough to prevent water from infiltrating (Figure 3c, dry (30 cm)). Such behavior was already observed for very hydrophobic soils (Dekker and Ritsema, 2000). The very strong hydrophobicity may result from the very high organic matter content (TOC = 90 g $kg^{-1}$), which is due to both organic activity (plants, microorganisms, etc.) and organic pollutant loads from runoff water (hydrocarbons).

## 3.3 Hydraulic characterization of the sedimentary layer and the sandy soil

Focus was put on intrinsic hydraulic soil characteristics of both sand and sediment without hydrophobicity. Thus, only experimental data (in laboratory and *in situ*) obtained for initially wet soil were considered.

Water retention curve shape parameters (n and m) were first estimated from the analysis of particle size distributions through BEST. Saturated and residual water contents ($\theta_s$ and $\theta_r$) and scale parameter for water pressure head ($h_g$) were then estimated by fitting equation (1) on the evaporation experimental data. Equation (1) was also fitted on experimental data with no *a priori* information on n and m (e.g. optimization variables set: $\theta_s$, $\theta_r$, n, m and $h_g$) (Table 1, all fitted). Fitting was performed using RETC (van Genuchten, 1991).

Hydraulic conductivity shape parameter $\eta$ was estimated from equation (2b). As indicated in section 3.2, the averages of the saturated hydraulic conductivities were estimated directly from steady state infiltration rates for wet sand and using BEST algorithm for the sediment.

The experimental data (points) and modeled (lines) characteristic curves are illustrated in Figure 4 and related hydraulic parameters detailed in Table 1. Hydraulic parameters estimated either by fitting all parameters or by BEST were comparable for the sand and in the same order of magnitude for the sediment for which small

differences on n, m, $\theta_r$ and $\eta$ were obtained. The greater difference in $\eta$ resulted from the sensibility of equation (2b) on m n product. Despite these differences, both fitted values and BEST calculated values allow accurate modeling of experimental water retention curves and lead to similar conclusions (Figure 4a). The sediment distinguishes from sand by both a higher saturated and residual water contents and a lower saturated hydraulic conductivity, around 50 times less than for the sand (Table 1, $K_s$).

Table 1 : hydraulic parameters related to the characteristic curves of the sediment and the sand

| Parameter | $\theta_r$ | $\theta_s$ | $h_g$ (cm) | $K_s$ (cm $min^{-1}$) | n | $\eta$ |
|---|---|---|---|---|---|---|
| Sediment (all fitted) | 0.318 (0.040) | 0.680 (0.008) | -39.9 (11.8) | (-) | 3.32 (0.90) | 4.97 (1.34) |
| Sediment (BEST) | 0.055 (0.042) | 0.680 (0.080) | -25.9 (0.1) | 1.65 $10^{-1}$ (3.84 $10^{-2}$) | 2.312 (< 0.01) | 9.40 (0.10) |
| Sand (all fitted) | 0.030 (-) | 0.354 (-) | -5.21 (-) | (-) | 2.77 (-) | 5.61 (-) |
| Sand (BEST) | 0.037 (-) | 0.354 (-) | -6.27 (-) | 7.81 (3.30) | 3.28 (0.06) | 4.57 (0.07) |

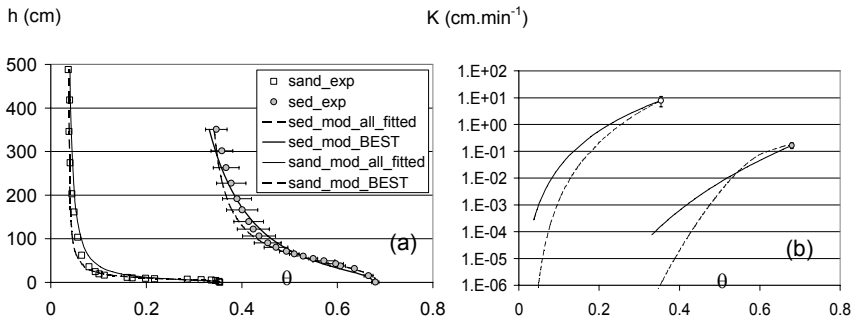


Figure 4 : Modeling (lines) and measured (points) sand and sediment hydraulic characteristic curves: water retention curves (a) and hydraulic conductivity curves (b).

## 4 CONCLUSION

The sedimentary layer accumulated in the infiltration basin of Cheviré was proved to significantly reduce the infiltration capacity of the sandy subsoil, even for the thickness of a few centimetres. This reduction was linked to the sediment hydraulic and physico-chemical characteristics. In particular, the saturated hydraulic conductivity of the sediment is around 50 times less than for the sand introducing a hydraulic resistance that explains part of the important decrease in infiltration capacity. Moreover, the physicochemical composition of the sedimentary layer (i.e. high organic matter content due to plant or organism development and organic pollutant loads) accentuates this hydraulic resistance by a strong hydrophobic behavior, in particular at low initial water contents.

These results, and in particular the complete unsaturated hydraulic characterization of both the sandy soil and the sediment, constitutes a material database useful for numerical modeling of the Cheviré basin. Such a modeling will help to understand the effect of the sedimentary layer on stormwater infiltration and pollutant transfer at the work scale and depending upon hydric and hydraulic conditions. Further research will

also be necessary to understand soil profile hydrophobicity and its effect on stormwater infiltration and pollutant transfer, in particular under dry conditions. At last, from a technical point of view, this study suggests that the settlement of sedimentary layers can greatly affect basin operation and confirms that stormwater must settle in a separate retention ponds before being infiltrated in order to minimize sedimentation in infiltration basins.

## 5 AKNOWLEDGEMENT

The authors would like to thank Laetita Letellier, Alice Biczysko, Sophie Ricordel, Béatrice Béchet and Veronique Ruban for their technical help and scientific discussions.

## REFERENCES

Braud, I, De Condappa, D., Soria, J. M., Haverkamp, R., Angulo-Jaramillo, R., Galle, S. and Vauclin, M. (2005). Use of scaled forms of the infiltration equation for the estimation of unsaturated soil hydraulic properties (*Beerkan* method). *Euro. J. of Soil Sci.*, 56, 361-374.

Brooks, R.H. and Corey, C.T. (1964). *Hydraulic properties of porous media.* Hydrol. Paper 3., Colorado State University, Fort Collins.

Buczko, U., Bens, O., Fischer , H., and Hûttl, R.F. (2002). Water repellency in sandy luvisols under different transformation stage in northeast germany. *Geoderma,* 109, 1-8.

Burdine, N.T. (1953). Relative permeability calculations from pore size distribution data. *Petr. Trans. Am. Inst. Mining Metall. Eng.*, 198, 71-77.

Chocat B., Bardin, J. P. and Gautier, A. (1999). Filtration devices for urban drainage: a 50-year experience in Lyons. *Am. Soc. Civ. Eng.Task Comm. Rep*., 181-195.

Clothier, B.E., Vogeler, I., and Magesan, G.N. (2000) The breakdown of water repellency and solute transport through a hydrophobic soil. *J. Hydrol.,* 231-232, 255-264.

Dekker, L.W. and Ritsema, C.J. (2000). Wetting pattern and moisture variability in water repellent Dutch soils. *J. Hydrol.,* 231-232, 148-164.

van Genuchten, M. Th., Leij, F.J. and Yates, S.R. (1991). *The RETC code for the quantifying hydraulic functions of unsaturated soils.* Technical Report, IAG-DW, 12933934, US salinity laboratory, Department of Agriculture, Agricultural Research Service, Riverside CA.

van Genuchten, M.Th. (1980). A closed form equation for predicting the hydraulic conductivity of unsaturated soils. *Soil Sci. Soc. Am. J.,* 44, 892-898.

Lassabatere, L., Angulo-Jaramillo, R., Soria Ugalde, J. M., Cuenca, R., Braud, I. and Haverkamp, R. (2006). Beerkan Estimation of Soil Transfer parameters through infiltration experiments – BEST. *Soil Sci. Soc. of Am. J.*, 70, 521-532.

Mataix-Solera, J. and Doerr, S.H. (2004). Hydrophobicity and aggregate stability in calcareous topsoils for fire-affected pine forests in southeastern spain. *Geoderma*, 118, 77-88.

Robichaud, P.R. (2000). Fire effects on infiltration rates after prescribed fire in northern rocky mountains forests, USA. *J. Hydrol.*, 231-232, 220-229.

Smith, R.E., Smetten, K.R.J., Braodbridge, P. and Woolhiser, D.A. (2002). *Infiltration theory for hydrology applications*. American Geophysical Union, Washington.

Valiron, F. and Tabuchi, J. P. (1992). *Maîtrise de la pollution urbaine par temps de pluie : Etat de l'Art*. Tec et Doc Lavoisier, Paris.

Wang, Z., Wu, Q.J., Wu, L., Ritsema, C.J., Dekker, L.W. and Feyen, J. (2000). Effects of soil water repellency on infiltration rate and flow instability. *J. Hydrol.*, 231-232, 265-276.